Silica glass structure generation for *ab initio* calculations using small samples of amorphous silica

Renée M. Van Ginhoven*
University of Washington, Seattle, Washington 98512, USA

Hannes Jónsson†
University of Washington, Seattle, Washington 98512, USA
and Faculty of Science, VR-II, University of Iceland, 107 Reykjavik, Iceland

L. René Corrales‡
Pacific Northwest National Laboratory, Richland, Washington 99352, USA
(Received 27 July 2004; published 28 January 2005)

Multiple small samples of amorphous silica have been generated and optimized using classical dynamics and the van Beest-Kramer-van Santen (BKS) empirical potential function. The samples were subsequently optimized and annealed using density functional theory (DFT) with both the local density and the generalized gradient approximations. A thorough analysis of the local and medium-range structure of the optimized samples obtained from the different methods was carried out. The structural characteristics obtained for the average of small systems each containing ca. 100 ions are compared for each of the different methods, and to the BKS simulation of a larger system. The differences found between the DFT and BKS simulations and the effects of volume relaxation on the structures are discussed. Fixed-volume samples are compared to neutron scattering data, with good agreement to 5 Å, the length limit of the sample sizes used here. It is shown that by creating multiple small samples, it is possible to achieve a good statistical sampling of structural features consistent with larger simulated glass systems. This study also shows that multiple small samples are necessary to capture the structural distribution of silica glass, and therefore to study more complex processes in glass, such as reactions.

DOI: 10.1103/PhysRevB.71.024208 PACS number(s): 61.43.Bn, 61.43.Fs

I. INTRODUCTION

Amorphous silica is the major component of importance in many applications, such as semiconductor devices,[1] optical fibers,[2] and waste confinement,[3] in addition to other commercial glasses.[4] The theoretical study of molecular-level processes in amorphous silica, such as chemical reactions and diffusion, requires the description of both the electronic and ionic degrees of freedom. Density functional theory (DFT), which provides a description of both the electronic and ionic degrees of freedom, has been shown to be a powerful tool to study molecular processes in the condensed state. However, DFT is subject to inherent limitations in system size, so studies are restricted to small samples. Because many processes of interest occur at the local molecular level, small samples can be acceptable. It is of interest to understand how well small simulated amorphous systems are able to describe the short- and medium-range structural features and their population and spatial distributions as compared to an extended amorphous system. Early classical simulations of amorphous silica were carried out in relatively small system sizes of the order of 10^2 atoms.[5,6] Subsequently, it was determined that larger systems were needed in classical simulations because of finite-size effects.[7] It has been nearly a decade since amorphous silica was first generated by DFT simulations with great success.[8] However, little has been done to address the issue of structure quality of small systems as compared to large systems. The goal of this work is to generate a good representation of the defect-free amorphous silica structure[9] appropriate for use in electronic structure studies, which effectively captures the statistical distribution of important structural features observed in larger simulated systems.

Previous calculations and simulations of crystalline, amorphous, and melt states of silica based on DFT with a plane wave basis set include studies of structure,[10,11] electronic properties,[8] thermodynamics,[12,13] infrared[14] and Raman spectroscopy,[15,16] defects,[17,18] excitons,[19,20] and the diffusion and reactions of water.[21] For some systems, such as crystals, the use of a limited system size is reasonable because there is little variation in the local structure. An exception for crystals would be for cases where defects and impurities play an important role. For liquids (ergodic systems), a small system size can work well because the sampling time is long enough that the system can sample many configurations and thus good statistical averaging is obtained. In contrast, a glass (a nonergodic system) is in any one of many possible network configurations that have nearly equal free energy. Generally, the study of amorphous systems requires the inclusion of a sufficient number of atoms to ensure that the distribution of structures is well represented, which is easily achieved by using large samples. A small sample is less apt to contain a full distribution of structural features. To ameliorate this shortcoming of small samples, multiple samples are prepared that as a group can contain representative distributions of the intermediate-range structure.[18]

The method described here has, to some extent, been used by others.[16,18,22] The basic approach is to first use classical dynamics based on an empirical interaction potential function to generate glass structures; then the resulting structures

are used in DFT molecular dynamics to determine structural, thermodynamical, mechanical, and other properties.

Variations on this approach include classical simulations on relatively large systems, large with respect to what can be done in an *ab initio* simulation, from which the smaller system is extracted.[11] This is reasonable for the liquid (melt) state that can quickly equilibrate, but can be computationally expensive if the equilibration of the liquid and the subsequent quench to the glass state are carried out with the *ab initio* simulation.[12,13] Alternatively, the glass quench is carried out in the classical dynamics simulation and then the structure optimized and annealed using *ab initio* simulation. Optimization can be carried out at constant volume[16,22] or at constant pressure, where the latter can be carried out by varying the periodic walls isotropically or anisotropically.[18] For small samples, technical issues arise when carrying out the glass quench during the classical simulations, due to the finite size of the system. In this work, we address some of these issues and employ techniques to evaluate the quality of the simulated systems.

In the present study, multiple small samples of amorphous silica were generated, each containing 72 atoms. Both classical dynamics and quantum mechanical approaches were used where the samples were first generated using classical dynamics, and then defect-free structures were further optimized and annealed using DFT. The method of sample generation is similar to that used by Benoit and co-workers,[16,22] who generated three separate amorphous samples by using three different cooling schedules. In the study presented here, the multiple samples were generated from separate random initial configurations, and then quenched with identical cooling schedules. The structural characteristics of the samples were thoroughly investigated to determine the extent to which the samples capture the characteristics of a larger glass. We observe that it is possible to generate a set of unique small glass networks that represent the distributions of the molecular structures in a larger simulated glass.

The bases of the structure analysis used to compare simulated samples are the molecular features of the silica network that represent the short- to medium-range order. The structure of silica glass is made up of silica tetrahedra, polymerized to form a network. The short-range order occurs at the level of the tetrahedra, and is described in the Si-O bond lengths and O-Si-O bond angles in a tetrahedron, and the Si-O-Si bond angles between connected tetrahedra. The medium-range structure is determined by the linking of these tetrahedral units, at the oxygen atoms which define the vertices, into more extended structures and rings. The network then consists of rings of different sizes that occur in a wide range of geometries with a distinct population distribution. The rings are in turn assembled into many possible conformations to make up the entire glass configuration. We have calculated bond length and bond angle distributions in both small and large samples, as well as ring size distributions and the orientation of adjacent tetrahedra.

The rest of this paper is organized as follows. In Sec. II, the methods used to generate the glasses are presented, beginning with classical glass-forming simulations, optimization with DFT, additional annealing with DFT, and generation of the larger reference glass system. In Sec. III, results are presented. First energy and density differences by sample are considered, then pair distribution functions for Si-O, O-O, and Si-Si, and the total distribution function as compared to experimental data. Next presented is a higher-order structural analysis, which includes O-Si-O angles, Si-O-Si angles, ring size distributions, torsion angle distributions, and tilt and twist between adjacent tetrahedra. In Sec. IV the results are discussed. Section V provides conclusions, and finally there is an Appendix with some additional information.

II. COMPUTATIONAL PROCEDURE

Multiple glass samples using systems consisting of 72 atoms (24 SiO_2 units) were generated using classical dynamics simulations with step cooling from $T=7000$ to 300 K in 140 ps using the van Beest-Kramer-van Santen[23] (BKS) empirical potential energy function. This cooling procedure, described in detail below, reliably produces a large percentage of glass samples free of configurational defects (see the Appendix). At the initial density of 2.20 g/cm^3, the simulation cell size is approximately 10 Å per side, large enough to describe range-I order, the majority of range-II order, and some aspects of range-III order of a glass.[24,25]

The BKS simulations where carried out using the DL_POLY software.[26] The low-temperature glass configurations obtained from the BKS simulations were then annealed by using first-principles calculations of the atomic forces. The DFT calculations were carried out using the Vienna *ab initio* simulation package[27–30] (VASP) with details described below.

A. Simulations using the BKS potential function

The glass configurations were generated by by first carrying out simulations at a high temperature for long enough time to equilibrate the melt and then step-cooling the silica liquid. The BKS potential has been used extensively to simulate both crystalline and amorphous silica, and has been shown to give a good description of defect-free bulk silica.[31,32] Each starting configuration consisted of 24 silicon atoms and 48 oxygen atoms placed randomly within the volume of the simulation cell. An exclusion radius of 3.1 Å for silicon-silicon distances, 2.5 Å for oxygen-oxygen distances, and 1.5 Å for silicon-oxygen distances were used to prevent overlap of particles. Periodic boundary conditions were applied, with the long-range electrostatic forces handled by Ewald sums.[33] A pathology in the BKS potential that can lead to unphysical collapse of ions at high temperatures and close distances was fixed by adding a close-range repulsive potential.[34] The short-range part of the potential was truncated at 4.63 Å, less than half the size of the simulation cell, without shifting the forces. Each configuration was thoroughly annealed at constant volume, with the density of the samples held fixed at 2.20 g/cm^3. This is an average density for fused silica.[32] Using a time step of 2 fs, each sample was equilibrated at 7000 K for 40 ps, and then step cooled to 6000, 5000, 3000, 1000, and finally 300 K, remaining at each temperature for 20 ps. The particle velocities were scaled every 20 time steps for 12 ps at each temperature and

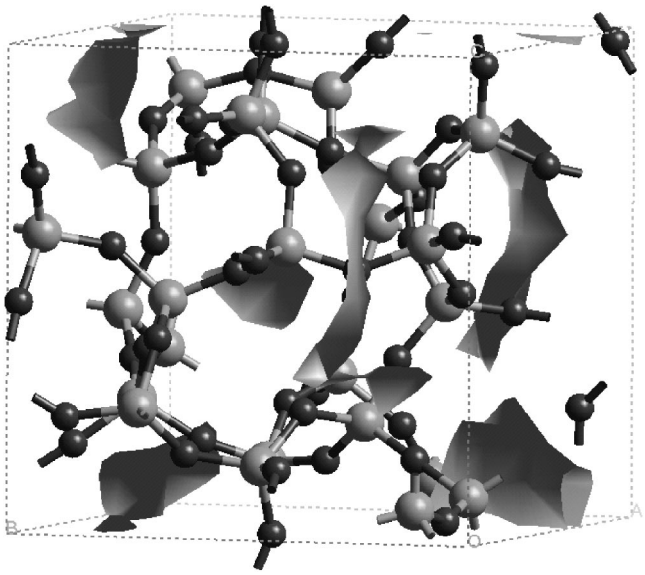

FIG. 1. One of the 72-atom glass samples used for further study in this work (glass 5). The larger, light gray spheres are silicon atoms, and the smaller, dark gray spheres are oxygen atoms. The medium gray surface shows the void space accessible to a probe of diameter 1 Å. In this sample, the network, and therefore the void space, is distributed relatively evenly over the volume of the simulation cell.

then run at constant energy thereafter. The overall cooling rate was on the order of 10^{13} K/s. This approach was used to generate 25 independent configurations. This quenching algorithm is similar to schedules used by others[35,36] and to those recommended in the literature.[37]

After the completion of the empirical glass-forming procedure, samples for use in this study were considered acceptable when they contained no coordination defects, because perfect coordination is desired to study the behavior of the pure system. Samples were also discarded if they contained any edge-sharing tetrahedra, or if there were large void spaces. The presence of more than two three-membered rings was correlated with the presence of large voids. Edge-sharing tetrahedra are considered to be strained structures, and should occur with low probability in a well-annealed glass.[38] Detailed description of structural features are presented in the Appendix. Figure 1 shows an example of a glass structure selected for this study. Out of the 25 samples generated, 18 met the acceptance criteria.

B. Optimization with plane-wave DFT

Ten glass samples were selected and further refined by additional relaxation and volume optimization by DFT. Calculations were performed using both local density approximation[39,40] (LDA) with the functional parametrized by Perdew and Zunger[41] and generalized gradient corrected (GGA) DFT calculations with the PW91 functional.[42] The ions were represented by Vanderbilt ultrasoft pseudopotentials,[43–46] and a plane-wave basis set was used, with an energy cutoff of 396 eV, and augmentation charge cutoff of 928 eV for the GGA and LDA. Due to the large number of calculations required, this work used only the Γ point for the Brillouin-zone integration. This was shown to be adequate in earlier work on quartz.[19]

The geometry minimizations were carried out using a convergence criterion of 0.01 eV $Å^{-1}$ for all interatomic forces. This tight criterion was necessary because the potential energy surface for silica was found to be rather flat. A convergence criterion of 10^{-4} eV was used for the electronic energy at each step in the optimization. Optimization of the structures was done using an iterative conjugate-gradient minimization scheme. A 30% increase in the number of plane waves was used for high-precision single-point calculations, as this was sufficient to converge the energy with respect to the plane-wave basis set.

Optimization of the cell volume was performed for each sample. A series of volumes that were larger or smaller than the initial density was made by scaling the box lengths and the atom positions. At each volume, the ion positions were fully optimized using both the LDA and GGA, and then high-precision single-point calculations were performed for the end geometries. In this way, smooth curves of energy versus volume were constructed, and the optimum volumes were found. For the BKS potential, each sample was subject to constant-pressure molecular dynamics using the Berendsen barostat at 300 K for 10 ps. The volume of the sample was then fixed to the average equilibrium volume and the system quenched to 0 K.

C. Annealing with DFT

The empirically produced samples were heat treated by DFT molecular dynamics (MD) simulation as follows. For temperatures of 1500 K and above, the Nosé thermostat[47,48] was used. For lower temperatures, a periodic scaling of the velocities was used for equilibration because the system temperature did not converge to the desired range when using the Nosé thermostat at less than 1000 K. Complete evaluation of the electronic energy was performed at each step, to 10^{-4} eV, which enabled the use of a relatively large time step of 1 fs.

The glass 1 sample was heated first to 3000 K, and held at this temperature for 4 ps. Vibrational movements of the atoms at this temperature were quite large, on the order of 1 Å or more. Structural analysis showed the breaking and reforming of the same Si-O bonds, with no net diffusion of the atoms.

The glass was cooled in steps to 2500, 1500, and 300 K, before quenching back to a minimum. The final quench yielded the same structure as the initial input. Several fast quenches from 3000 K directly to a minimum, from statistically independent parts of the 3000 K run, also led to the original structure.

Glass 2 and glass 3 were also annealed at 3000 K, for 3 ps each. In both of these glasses a silica tetrahedral group was able to rotate, leading to some minor change in the network structure. In both cases, the rotation involved only a small region of the network. The rest of the atoms experienced significant vibrational motion, as in glass 1, but did not undergo rearrangement. For both glasses, quenching to a

minimum structure from different times in the run led either to the original starting structure for each glass, or a higher-energy structure with a dangling oxygen (only one bond), and a corresponding undercoordinated silicon atom adjacent to the rotated tetrahedral group.

Ab initio MD simulations were done on glass samples 4–10 at 300 K for 2 ps. In each case, the subsequent quench to 0 K led to the initial starting structure. Attempts were made to use accelerated methods, such as the activation/relaxation technique[49] (ART) for the annealing process in DFT. In the ART, the system is driven toward a nearby saddle point and then optimized to a new minimum on the potential energy surface. With the ART, glass 1 was able to visit neighboring states, but these states were high-energy defect states, rather than independent perfectly coordinated states. It is possible that after repeated applications of the ART, the system could have found a more stable, defect-free state, but this was not pursued. The efficacy of the ART may be affected by the size of the region allowed to rearrange. Theories on glass aging[50] indicate that within a glass, transformation of larger regions may lead to lower-energy states, while transformation of smaller regions can lead to higher-energy states. Results of the high-temperature annealing and the ART simulations indicate that the generated systems are in relatively deep local minima, and significant atomic rearrangement is required to decrease the system energy any further.

D. Generation of larger reference glass system

The periodic boundary conditions and the small system size used in this study introduce constraints that are not present for larger-scale simulations. To test how well the small systems capture the characteristics of a larger glass, the structures of the small glasses were compared with a larger sample.

The larger glass system was made up of 1479 atoms, or 493 SiO_2 units. It was prepared by the same classical annealing methods as the smaller samples, using the same classical potential (the BKS potential) with the exception that the cutoff length was set to 9 Å. The sample was quenched from the melt in two ways; the first at constant volume, such that the density was 2.20 g/cm^3; and the second at constant pressure using the Berendsen barostat.[51] The *NPT* run resulted in a glass that was 2.33 g/cm^3, 6% denser than the *NVT* run. The 1479-atom glass contained about 1% defects, in the form of overcoordinated or undercoordinated atoms. The coordination number was determined by counting atoms at less than a specified cutoff distance that defines bonding between atom pairs. The cutoffs used to define bonding were $r_{Si\text{-}Si}=2.5$ Å, $r_{Si\text{-}O}=1.9$ Å, and $r_{O\text{-}O}=2.0$ Å. No O-O or Si-Si bonds were found. About 1% of the rings found in the system were three-membered rings. This population of defects and small rings is typical for the types and amounts of defects found in samples generated using the BKS potential.[31] The large simulation results are used to determine the quality of the small glass samples as a group. The ability of the BKS potential to generate good glass structures has been shown elsewhere.[31,52,53]

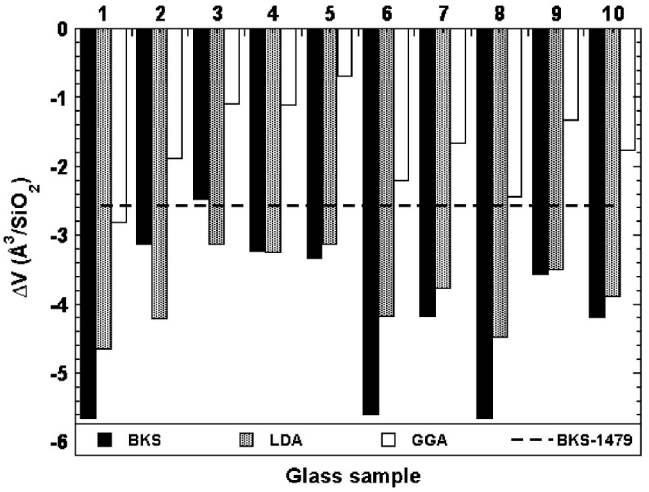

FIG. 2. The change in volume, in $Å^3$, for each glass sample after volume optimization or relaxation using the BKS potential, DFT-LDA, and DFT-GGA. Results for the BKS potential are shown in black, LDA are shown in gray, and GGA in white. Every sample decreased in volume. For most samples, volume relaxation with the BKS potential resulted in the greatest change. The relative trend for the LDA and GGA was similar, with the LDA leading to significantly greater change (and thus smaller cell sizes) for each glass.

III. RESULTS

A thorough analysis of the structural characteristics of the ten small glass samples was carried out, and compared to the same characteristics of the larger glass. For any given samples, optimization using different potentials did not change the connectivity of the network, but other structural characteristics were affected. Distributions of the Si-O bond lengths, first O-O and Si-Si pair distributions, the O-Si-O and Si-O-Si bond angles, and the torsion angle and ring size distribution were determined. The ring sizes are given in terms of the number of silicon atoms in a ring, so for example a ring with six Si and six O atoms is considered to be a six-member ring. Where available, data were compared to experimental quantities. The average total distribution functions (TDF's) of the optimized structures were compared to the TDF of a larger glass sample, and to experimental neutron diffraction data.[54]

In addition, analysis was done at the the level of the tetrahedral unit. The intra-tetrahedral tilt and twist angle distributions were examined. Descriptions of these quantities are given below.

A. Energy and density differences by sample

Figure 2 shows the histogram of the change in volume per SiO_2 unit for the ten samples volume optimized (VO) using the BKS potential, LDA, and GGA, compared to the change in volume in the larger glass sample. The change in volume per SiO_2 unit is reported with respect to the initial fixed volume of 2.20 g/cm^3. Every sample decreased in volume. The relative trend for the LDA and GGA was similar, with LDA leading to significantly greater change (and thus smaller cell sizes) for each glass. The density after relaxation

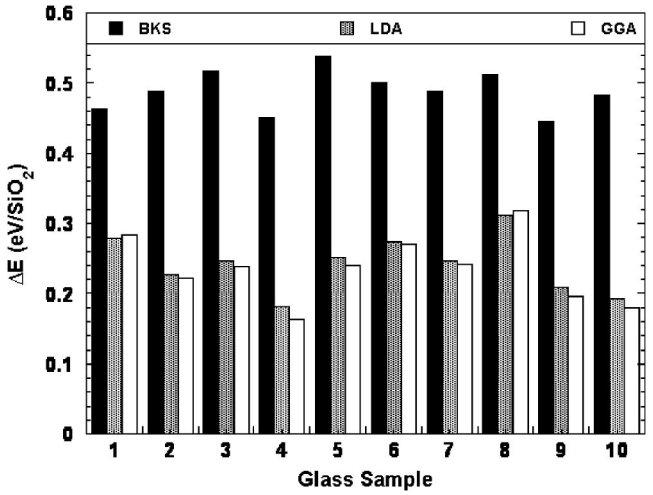

FIG. 3. The energy of each volume-optimized sample as compared to quartz. The data representation is the same as in Fig. 2. The relative energy difference is significantly greater for the BKS potential than for the DFT methods. The trend in energy is very similar for the LDA and GGA, with the difference from quartz being slightly larger using the LDA for eight out of the ten samples studied. Energy for DFT-optimized quartz is from work by Demuth *et al.* (Ref. 55).

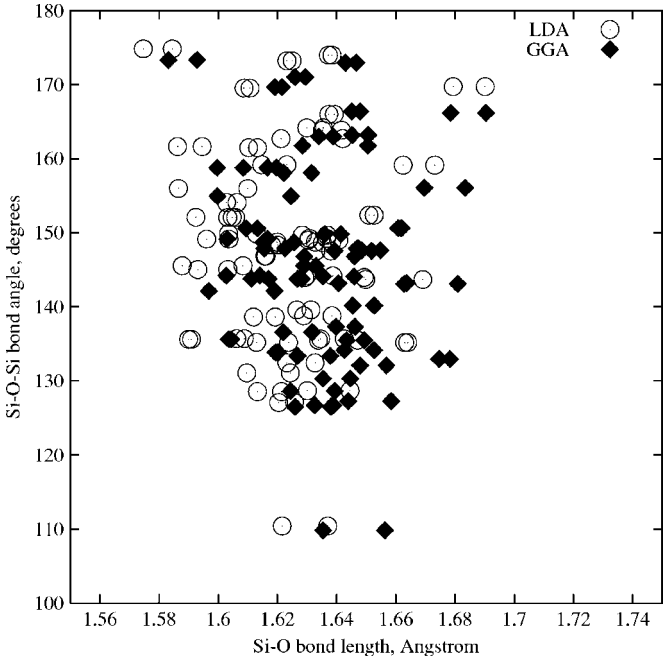

FIG. 4. Comparison of the scatter of Si-O bond length versus Si-O-Si bond angle for glass 6 optimized using the LDA and GGA with the volume held fixed at 2.20 g/cm^3. The open circles indicate the data for the LDA, and the filled diamonds for the GGA. It is apparent that the system undergoes a nearly uniform shift to shorter bond lengths and wider Si-O-Si bond angles in going from the GGA to the LDA.

with DFT-LDA ranges from 2.37 to 2.45 g/cm^3, while optimal densities obtained with DFT-GGA ranges from 2.24 to 2.33 g/cm^3. This density difference, of about 6.5%, is consistent with previous DFT calculations performed on a wide variety of crystalline silica polymorphs, in which the optimal cell volumes are found to be smaller for the LDA than the GGA.[55] LDA calculations result in densities that are about 1% higher than experimental densities for low-density crystalline silica polymorphs.[55] The relative volume change of each sample was qualitatively the same using the BKS potential. The density changes were similar in magnitude to the results obtained with the LDA, with a greater spread in volume, 2.33–2.52 g/cm^3, and higher average density. As pointed out above, the density for the larger-sample BKS potential also increased. Note that the density of silica obtained from simulations is strongly dependent on the short-range potential cutoff and whether or not corrections to the energy at the cutoff are included.[32,34]

Figure 3 shows the histogram of the relative energy for the ten samples volume optimized using the BKS potential, the LDA, and the GGA. The relative energies per SiO_2 unit of the optimized structures are compared to one another where the reference energy is that of quartz calculated using the same method. The trend in relative energy is very similar for the LDA and GGA, with the difference from quartz being slightly larger using the LDA for eight out of the ten samples studied. Optimization using the BKS potential results in a different trend of relative energy. There is no clear correlation between the relative sample energy and optimum sample density.

Previous work has shown that for fixed identical volumes, optimization with the LDA or GGA results in nearly identical coordinates for crystalline polymorphs of silica.[55] This is not the case for amorphous silica. Figure 4 shows the scatter of Si-O bond lengths versus Si-O-Si angles plotted for both LDA and GGA optimized glass 6 at a fixed volume of 2.20 g/cm^3. It is apparent that the system undergoes a nearly uniform shift to shorter bond lengths and wider Si-O-Si bond angles in going from the GGA to the LDA.

B. Pair distributions

The average Si-O, O-O, and Si-Si pair distribution functions are evaluated as experimental values derived from neutron scattering experiments to produce total distribution functions. Individual features are discussed below. Data are shown in Table I.

Figure 5 shows a comparison of the average silicon-oxygen bond length distributions of the ten 72-atom glass samples with the bond length distribution for the 1479-atom glass. The bond length distributions for the large and small configurations quenched with the BKS potential are quite similar. Results for the LDA at fixed volume are similar to the BKS potential. The DFT-GGA results give slightly longer bond lengths, by about 0.01 Å on average, than the BKS potential. This is due to the difference in interatomic forces, rather than the size of the system. Optimizing the cell volume, or allowing the cell volume to relax resulted in slightly shorter average bond lengths for all the configurations, and narrower bond length distributions, for the small systems. This effect was most pronounced for DFT-LDA, which also had the greatest degree of change in the volume.

Figures 6 and 7 show the first peak in the O-O and Si-Si pair distribution functions, respectively. Optimization

TABLE I. Short-range structural characteristics of glass samples. The average pair distances are reported with standard deviation for the simulated values.

Glass	ρ (g/cm^3)	$R_{\text{Si-O}}$ (Å)	$R_{\text{O-O}}$ (Å)	$R_{\text{Si-Si}}$ (Å)
72-atom average				
GGA	2.20	1.632(0.020)	2.67(0.104)	3.105(0.114)
GGA-VO	2.24–2.33	1.626(0.018)	2.67(0.104)	3.073(0.114)
LDA	2.20	1.621(0.022)	2.65(0.109)	3.100(0.113)
LDA-VO	2.37–2.45	1.607(0.016)	2.64(0.107)	3.030(0.120)
BKS	2.20	1.619(0.019)	2.64(0.119)	3.122(0.103)
BKS-*NPT*	2.33–2.52	1.609(0.018)	2.63(0.121)	3.059(0.108)
1479-atom sample				
NVT	2.20	1.616(0.024)	2.64(0.116)	3.104(0.106)
NPT	2.33	1.609(0.024)	2.63(0.118)	3.072(0.111)
Expt.	2.19–2.31	1.61	2.66	3.077

of the volume causes a shift toward closer distances, and a slight narrowing of all the first-neighbor distributions. At fixed volume, O-O distances are closest for the LDA. Distributions are widest for the BKS potential. Differences in the Si-Si distances are extremely small. Distributions for the larger glass are slightly wider than for the small samples using any method.

Optimization of the volume causes a shift toward closer Si-Si distances. This is expected due to the smaller cell volumes after optimization. This structural characteristic can be most easily related to the Si-O-Si bond angle distribution (BAD); however, this angle is also affected by bond lengths, and changes in local torsion or twisting between neighboring silica tetrahedra.

1. Total distribution function: Comparison with neutron scattering data

Total distributions functions were constructed for each silica sample at fixed density of 2.20 g/cm^3, with peaks for the structural data broadened using the formulation suggested by Wright.[25] Figure 8 shows a comparison of the constructed results with neutron scattering experiments.[25,54] The average TDFs for the small samples were truncated at a distance of 5 Å.

The fit to the experimental data for the 1479-atom glass is similar to results obtained for other simulations, with an R_x factor of about 8.[54] As the composite curves for the smaller glasses may only be considered to 5 Å, the comparison of the TDF to experimental data may only be considered qualitatively at this time. It is evident that the average TDF for the 72-atom systems is more similar to the TDF for the 1479-atom glass than to the experimental data. This may indicate that there is some underlying bias in the structures due to the choice of the initial empirical potential, the small size of the systems, and the glass-cooling algorithm employed. Nevertheless, the results indicate that the volume-optimized samples have too-close distances for both the O-O and Si-Si peaks.

C. Higher order analysis

The average O-Si-O, and Si-O-Si bond angle distribution, Si-O-Si-O torsion angle distribution (TAD), and ring structure are examined and compared with the results for the larger glass. These structures may be inferred experimentally from neutron scattering, and Raman spectroscopy, but are challenging to measure directly. Data for the O-Si-O and Si-O-Si BADs are shown in Table II. Analysis is also performed at the level of tetrahedral structural units. Individual features are described and discussed below.

1. O-Si-O bond angle distribution

Figure 9 shows the average oxygen-silicon-oxygen BAD of the small glasses, and the quenched glass 1479. These curves are similar for all potentials, and large and small samples. Optimization of the volume leads to a slight narrowing of the O-Si-O BAD, but the average value is relatively insensitive to changes in the volume (see also Table II). Among the small systems, the average BAD is slightly wider for the 72-atom systems optimized with the BKS potential. This widening is likely to be related to the spherical nature of the potential. This angle is more flexible than in DFT, with directionality being derived only by electrostatic repulsion between the fixed-charge oxygen atoms. The BAD is wider for the larger sample than the small systems due both to the potential and to the presence of some coordination defects. The tails in the distribution of the large sample are not represented by the small samples used in this work due both to the small number of samples, and the deliberate selection of perfectly coordinated samples. It is also possible that the small size restricts the conformation of the network.

2. Si-O-Si bond angle distribution

The Si-O-Si BADs are shown in Fig. 10. In the linked-tetrahedra model of silica, these angles may be thought of as the hinges between adjacent silica tetrahedra groups. The Si-O-Si angle distribution begins to show the intermediate-range structure of the system, because it is the angle between

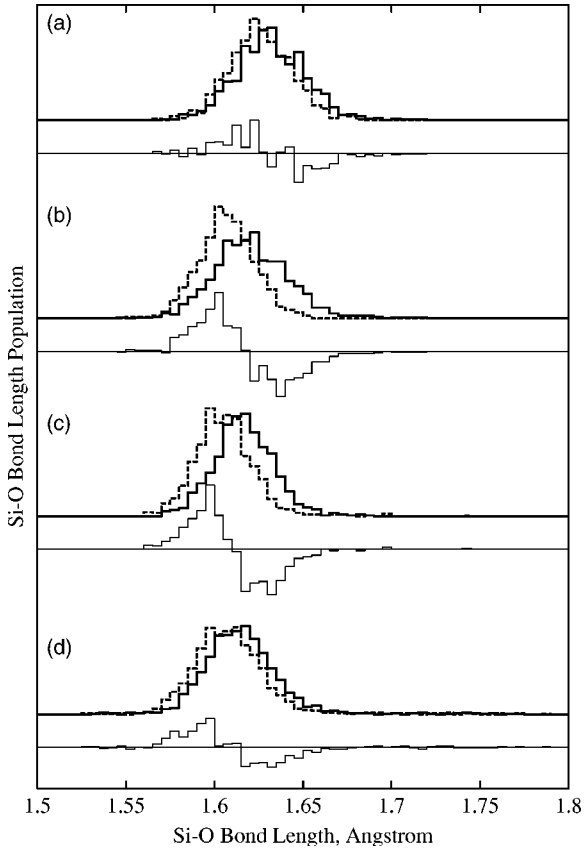

FIG. 5. Comparison of the average silicon-oxygen bond length distribution for the ten 72-atom systems used in this study with the silicon-oxygen bond length distribution of a quenched 1479-atom configuration. The top three curves correspond to the average structure of the ten small systems optimized using (a) the DFT-GGA, (b) the DFT-LDA, and (c) the BKS potential. The bottom set of curves (d) is for the 1479-atom glass sample for which the volume was allowed to relax, during a *NPT* classical MD run using the BKS potential, and for the 1479-atom sample held at a fixed density of 2.20 g/cm^3. The thick solid lines show the bond length distribution for systems held at fixed density 2.20 g/cm^3, while the dashed lines show the same distributions for systems with relaxed or optimized volume. The thin lines under each pair of distributions show the difference in the distributions $\mathcal{P}(V_{opt})-\mathcal{P}(V_{2.2})$.

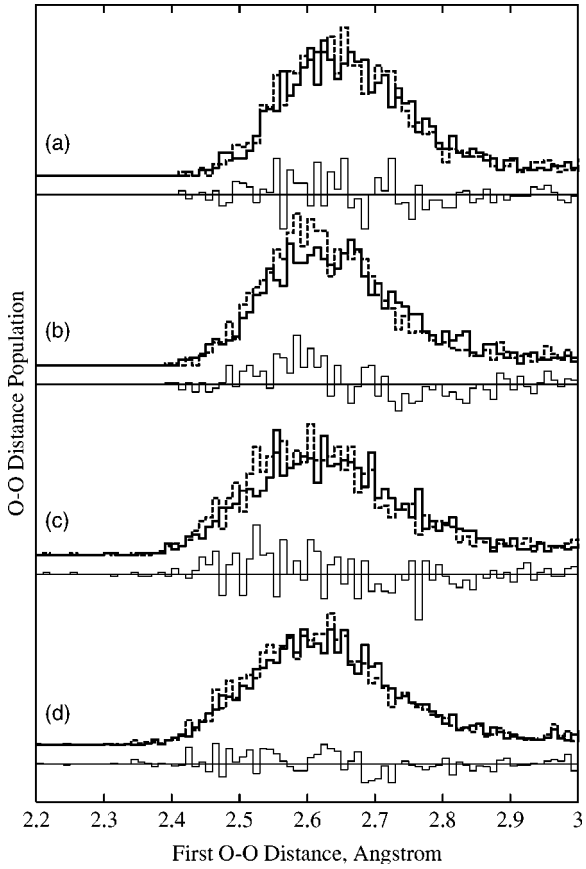

FIG. 6. The first O-O distance in the pair distribution function. The arrangement of curves is the same as for Fig. 5. Optimization of the volume causes a shift toward closer O-O distances, and a slight narrowing of the distribution.

adjacent silica tetrahedra, and participates in ring structure. The data show that the Si-O-Si BAD is sensitive to changes in the cell volume (volume relaxation), as well as the potential used.[31] The Si-O-Si BAD for the small glasses quenched using the BKS potential is very similar to that of the larger glass. Use of DFT, especially the GGA, results in smaller average Si-O-Si angles even before optimization of the volume (see Table II). The BAD found using DFT-LDA is shifted slightly to smaller angles, and the BAD found using DFT-GGA is shifted even more than for DFT-LDA, consistent with the longer GGA Si-O bond lengths.

With volume relaxation, the average Si-O-Si bond angle was consistently shifted toward smaller angles, and the distribution slightly narrowed. This effect was greatest when the samples were optimized using DFT-LDA, which is likely partially due to the greater sample density (smaller optimum cell size) obtained with the LDA.

3. Ring size distribution

One way to quantify the connectivity of a network solid is through analysis of minimum (primitive) ring structures. For silica, an *n*-ring is defined counting only the participating silicon atoms (see the Appendix). Quartz is composed of six-membered and eight-membered rings, while fully amorphized silica is expected to have a peak at the six- and seven-membered rings.[56] Analysis of the ring structure of each sample was done using the method of Yuan *et al.*[56,57] The maximum ring size in the search was set to 19 silicon atoms. Figure 11 shows the ring size distribution (RSD) for each of the ten 72-atom samples used in this study. The dramatically different ring distributions for the ten glass samples show that the connectivity of each sample is significantly different. This selection of different connectivities is one way to try to sample a selection of the many local structures which are possible for a larger system. Since optimization with different potentials did not involve any changes to the connectivity, the ring structure is unchanged as well. Glasses 4, 6, and 10 show peaks at six-member and eight-member rings. The high proportion of six- and eight-membered rings in glass 6 could be considered an indication of incomplete melting, or crystalline character in a larger sample; however, examination of other structural characteristics does not reveal crystalline character (see Fig. 4). In addition, the presence of

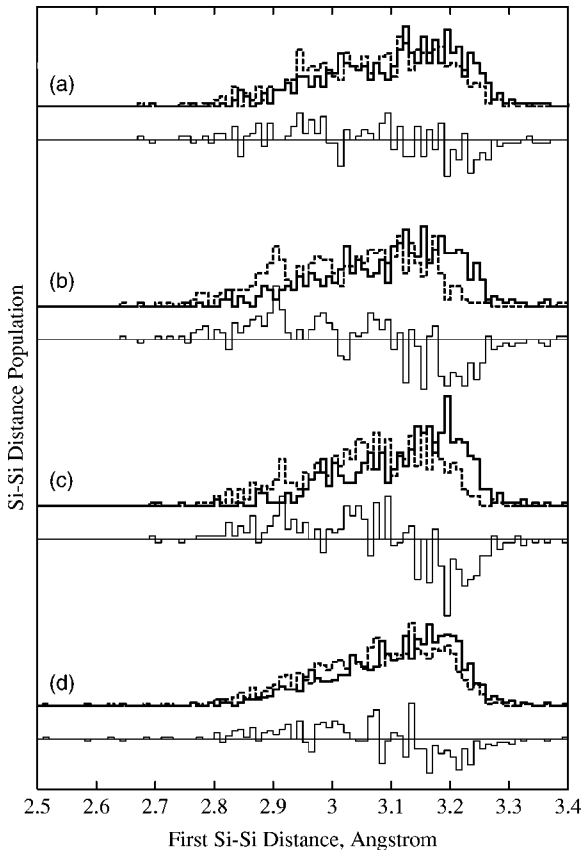

FIG. 7. The first Si-Si distance in the pair distribution function. The arrangement of curves is the same as for Fig. 5. Optimization of the volume causes a shift toward closer Si-Si distances. This is expected due to the smaller cell volumes after optimization.

significant population of other sized rings prevents the sample from being crystalline. For the collection of small samples, regularity in the ring size distribution was not used as a criterion to eliminate samples.

Figure 12 shows a comparison of the combined RSDs of the ten 72-atom samples with the RSD of the 1479-atom glass. The combined RSD has peaks at six-member and eight-member ring size, and is narrower than the RSD for the larger glass system. In particular, the tail of larger ring sizes is absent. It is clear that large rings are unavoidably underrepresented by small systems. The largest ring found in any of the small samples is a 13-ring. The three-membered rings are also underrepresented. The overall distribution of intermediate-sized rings is similar to that of the larger sample. The disproportionate representation of six-rings and eight-rings is due almost entirely to the influence of glass 6. Exclusion of glass 6 (see Fig. 13) yields a combined RSD with the peak at seven-membered rings.

4. Distribution of torsion angles

Figure 14 shows the average torsion angle distribution of the 72-atom glasses and 1479-atom glass. The torsion angle is defined as the Si-O-Si-O angle between series of bonded atoms, as by Yuan and Cormack.[53] Similar to the results shown in the same reference, there are peaks at 60°, and at

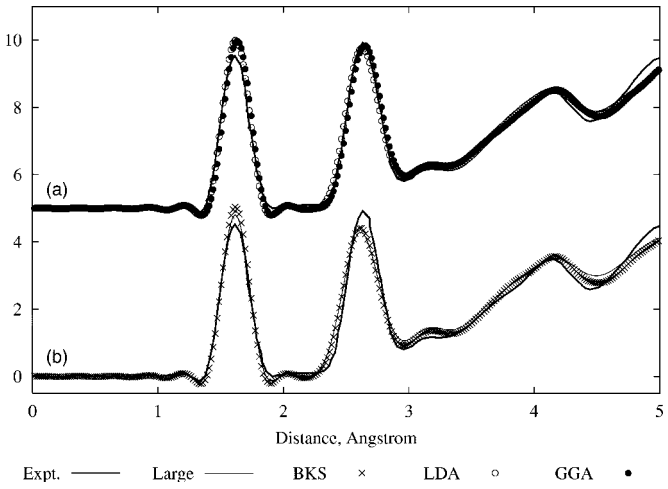

FIG. 8. Comparison of the constructed total distribution function of the ten 72-atom samples (averaged) and 1479-atom sample to experimental data (Wright *et al.*, Refs. 25 and 24). All data are for fixed density at 2.20 g/cm^3. The thick solid line shows the TDF from neutron scattering experiments. In (a), average DFT results are compared to experimental data, with the LDA represented by open circles, and the GGA by solid circles. The results using the BKS potential are shown in (b). The thin solid line is the TDF for the 1479-atom simulation, and the × marks are the data for the average of the small samples.

180°, which are related to the preference of the sample to be in a *trans* configuration, due to repulsion between oxygen atoms on neighboring silica tetrahedra. The TADs are quite noisy, and no significant differences can be seen between samples optimized with different methods, or between volume-optimized and fixed-volume results. It can be said qualitatively that the peak around 60° is more pronounced for the smaller samples as compared with the larger sample.

5. Analysis at the level of the tetrahedral unit

Due to the relative rigidity of the silica tetrahedra, shown by the results for the O-Si-O BAD above, it is useful to determine the relative conformations given by the tilt and

TABLE II. Angle distributions for glass samples. The average O-Si-O and Si-O-Si angles are reported, with standard deviation.

Glass	O-Si-O (deg)	Si-O-Si (deg)
72-atom average		
GGA	109.48(5.52)	146.76(13.88)
GGA-VO	109.47(5.20)	144.46(14.12)
LDA	109.47(5.79)	148.77(13.87)
LDA-VO	109.46(5.01)	143.43(14.48)
BKS	109.41(6.92)	152.24(12.91)
BKS *NPT*	109.34(7.47)	146.51(13.59)
1479-atom sample		
NVT	109.36(8.01)	149.91(14.35)
NPT	109.34(7.25)	147.78(14.26)

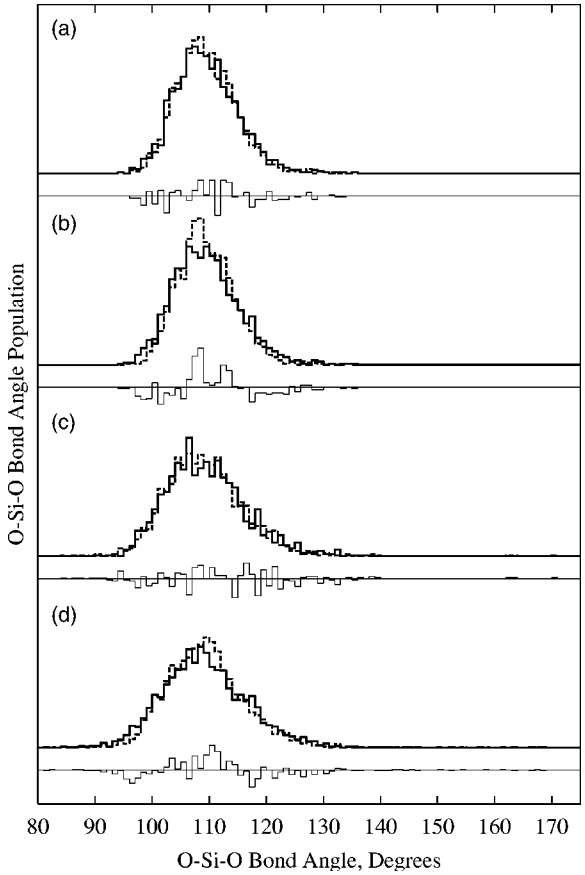

FIG. 9. Comparison of the average oxygen-silicon-oxygen bond angle distribution for the ten 72-atom systems used in this study with the oxygen-silicon-oxygen bond angle distribution of a quenched 1479-atom configuration. The arrangement of curves is the same as for Fig. 5. Optimization of the volume leads to a slight narrowing of the BAD, but the average value is relatively insensitive to changes in the volume (see also Table II.) This distribution is similar across potentials, although slightly wider for the 72-atom systems optimized with the BKS potential.

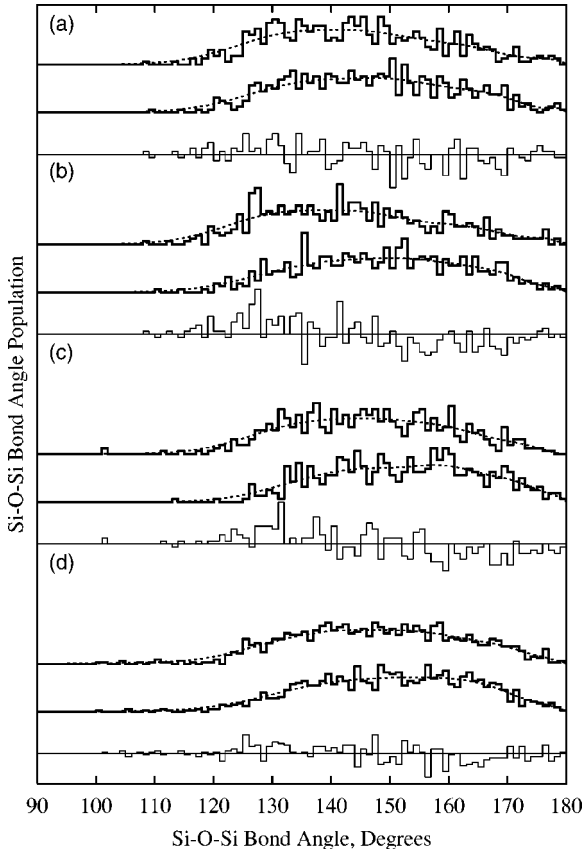

FIG. 10. The silicon-oxygen-silicon bond angle distributions of the ten 72-atom systems used in this study and a larger, 1479-atom configuration. For each pair of curves in bold, the top shows data for the volume-optimized samples, while the other shows data for fixed-volume samples. The dotted lines are a spline fit to the data, and are intended as a guide to the eye. The ordering of curve sets is the same as for Fig. 5. In all cases, relaxation of the volume resulted in a slight shift of the BAD to narrower angles. This shift is most noticeable for the 72-atom samples optimized with the BKS potential, and with the LDA. At fixed volume, use of DFT, especially the GGA, resulted in smaller average angles before optimization of the volume (see Table II).

twist between neighboring tetrahedra. Figure 15 illustrates the structure of a small amorphous silica sample shown in the polyhedral representation. Each tetrahedron is centered on the position of a silicon atom, with oxygen atoms at each vertex.

The tetrahedral tilt angle is defined as the O-O-O angle between linked tetrahedra, as shown in Fig. 16. Figure 17 shows the tetrahedral tilt distribution (TLD) for each set of glass samples. The tail at lower angles and the definite shoulder in the smaller sample results suggest that there may be a secondary peak. A fit of two Gaussian functions yields peaks at around 90° and 140°.

The twist between tetrahedra is defined as the torsion angle O-Si-Si-O, using the vector between neighboring silica tetrahedra as shown in Fig. 18. The tetrahedral twist distributions (TWDs) are shown in Fig. 19. The TWD shows peaks at 60° and 180° which are more clearly delineated than in the TAD presented above. These peaks are indicative of the repulsion between next-nearest-neighbor oxygen atoms. The TLD and TWD are strongly constrained in small ring structures, due to geometrical requirements.

IV. DISCUSSION

Comparison of the composite structure of an ensemble of small systems with the structure of a larger simulated system is valid because the convergence of structural properties with system size can be attributed to statistically capturing the key features of the large number of possible arrangements of the medium range structure. We have shown that the representation of the statistical distribution of structures can be achieved with an ensemble of small samples. For individual samples, finite-size effects have shown that silica glass is best studied by computer simulations using large system sizes.[7] This implies that studies of amorphous systems using techniques that require small system sizes are made possible by employing multiple small samples.

This work shows that one of the most interesting structural characteristics to capture is the ring size distribution. The ring distribution is relatively straightforward to deter-

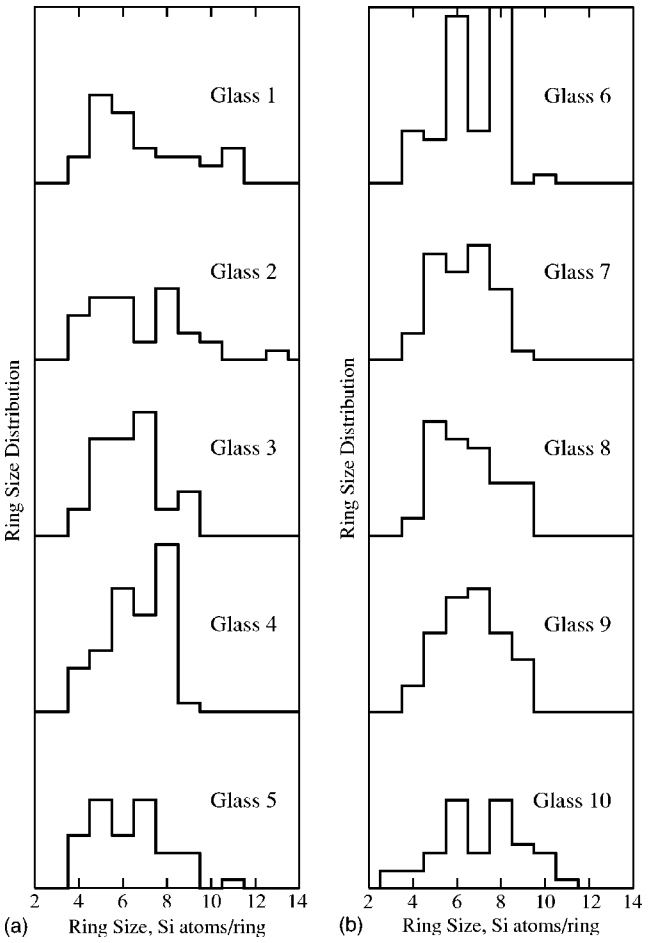

FIG. 11. Ring size distributions for glasses 1–10. The dramatically different ring distributions for the ten glass samples show that the connectivity of each sample is significantly different. The high proportion of six- and eight-membered rings in glass 6 would be considered an indication of incomplete melting, or crystalline character in a larger sample; however, examination of other structural characteristics does not reveal crystalline character (see Fig. 4) and this sample was not discarded.

mine quantitatively in atomic-level simulations. However, ring distribution is challenging to determine quantitatively by experiment. In Raman spectroscopy, small-sized rings may be detected, but larger rings are not easily distinguishable.[58] It can be important to match at least the small-ring-structure population because the increase in concentration of small-sized rings is correlated with enhanced reactivity of the silica structure.[59,60] [Note that only one sample with three-membered rings was included in this study (glass 10), while all samples contained four-membered rings.] Experimentally, the ring distribution, and the occurrence and concentration of coordination defects, may be controlled by the glass-forming history.[59,61] Some control of defect populations during annealing has also been shown to be possible in computer simulations.[32,62]

With the small samples, we have shown that it is possible to form a variety of significantly different structures using the same glass simulation algorithm. This is uniquely different from using the melting, cooling, and annealing algorithms generally used to control structure, and the difference can be attributed to the small sample size. This work shows that a variety of intermediate-range structure can be obtained without attempting to control the cooling rate, in contrast to other recent work.[16,22] Care must be taken in sample selection because the average ring size distributions can be biased artificially.

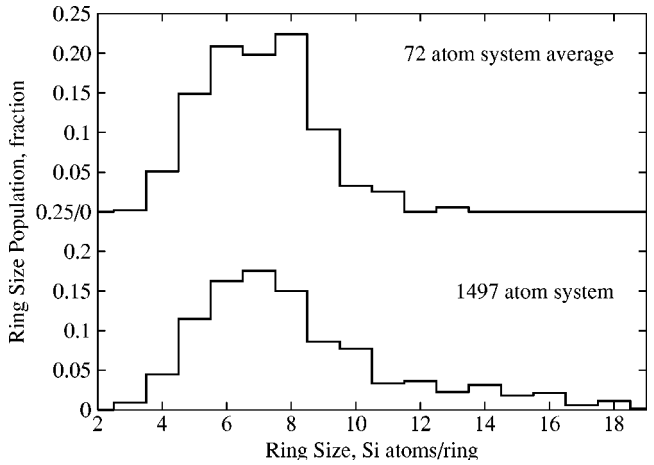

FIG. 12. Comparison of the ring size distribution averaged over ten 72-atom glasses and of a quenched 1479-atom glass configuration. The top curve shows the composite RSD for the ten 72-atom systems. The second curve shows the RSD for the larger glass sample.

Samples with significantly different ring structures may have indistinguishable features in the short-range part of the TDFs. The pair and angle distribution functions, given by the Si-O, O-O, and Si-Si distances, O-Si-O and Si-O-Si bond angles, and the torsion, tilt, and twist angles, show that the selected sample ensemble has good agreement in the peak positions and widths as compared to a large simulated sample. The sample ensemble used in this work did not include defects that may contribute to the tails of the distributions of distances and angles observed in the larger sample. It is conceivable that more samples that contain three-membered rings should have been included in this study.

By attempting to anneal structures to some other, lower-energy configuration it was determined that the structures formed by our primary method, as described above, are highly stable. It is possible that the system supercell size used is smaller than what might be needed to effect any simple transformations to other stable configurations.

The Si-O bond is generally considered to have partial ionic character coupled with an otherwise covalent bond. The directional nature of the covalent bond should be seen in

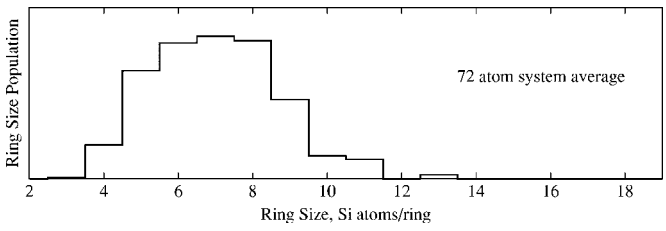

FIG. 13. The averaged small-sample RSD excluding glass 6.

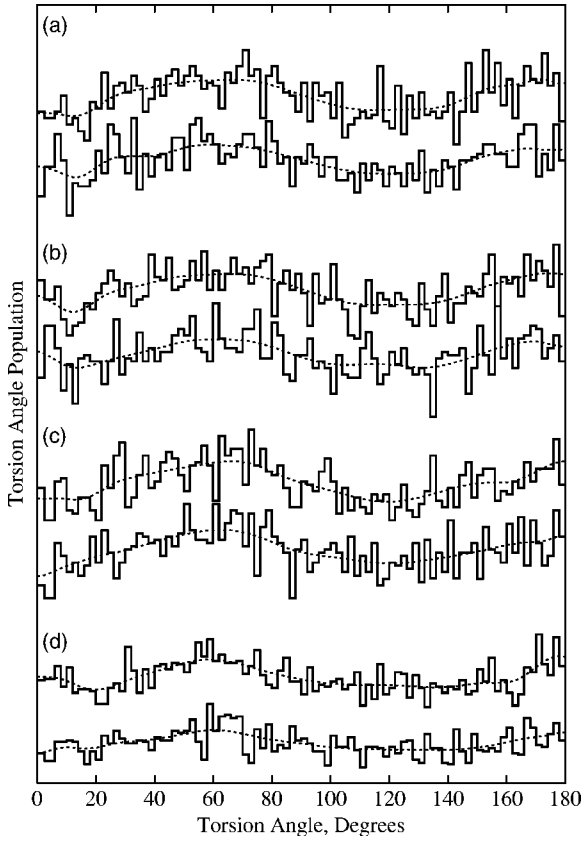

FIG. 14. The average torsion angle distribution of the 72-atom glasses and of the 1479-atom glass. The torsion angle is defined as in Yuan and Cormack. (Ref. 53). The data are presented in the following order: (a) GGA, (b) LDA, (c) BKS, and (d) 1479-atom sample (BKS potential). The upper of each pair of curves shows data for volume-optimized samples. The dotted lines are intended as a guide to the eye. The TADs are quite noisy, and no significant differences can be seen between samples optimized with different methods, or between volume-optimized and fixed-volume results, and therefore no difference plots are shown.

the width of the O-Si-O bond angle of the highly directional bonds that make up the silicon tetrahedron. The differences in the O-Si-O BAD seen between DFT and the BKS potential can be attributed to the *ab initio* method better representing the directional nature of the Si-O bond. The BKS potential is spherical and achieves tetrahedral structure through a strictly repulsive interaction between oxygen atoms. In contrast, the DFT methods are able to describe the directional orbitals involved in bonding. The difference is clearly seen in the width of the O-Si-O angle distribution (see Fig. 9 and Table II), which is narrower for DFT methods than it is for the BKS potential, as revealed by the standard deviation of this bond angle.

The Si-O-Si BAD for a crystal consists of discrete bond angles. In contrast, for a glass the distribution is broadened because this bond angle is associated with the ring size population and their conformations. The differences in going from the BKS potential to DFT are minimal and unlike the O-Si-O BAD no obvious contribution due to directional character from a covalent bond is seen for the Si-O-Si BAD. Upon optimization, the LDA results in shorter Si-O bonds and smaller average Si-O-Si bond angles than the GGA, but no obvious changes in the widths of the distributions are evident as determined by the standard deviations shown in Table II. In all cases, in going from the nonoptimized to the optimized structures, the average Si-O-Si bond angle decreases.

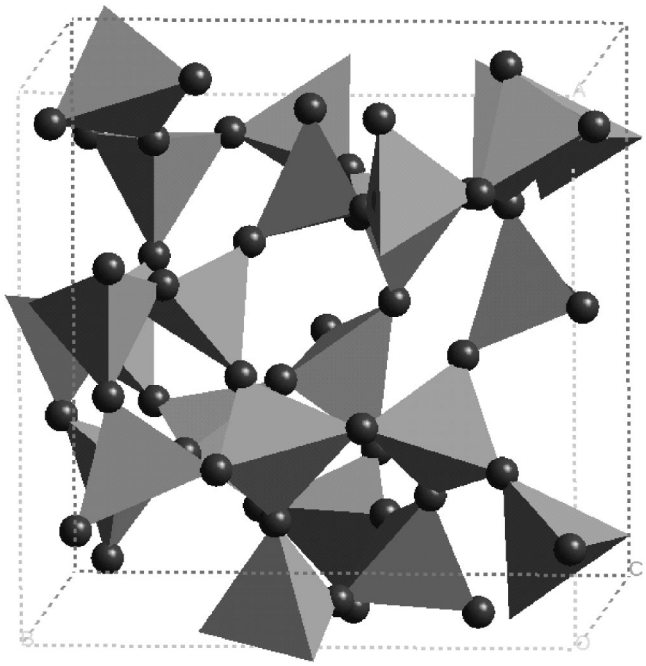

FIG. 15. The structure of a small amorphous silica sample, shown in the polyhedral representation. Each tetrahedron is centered on the position of a silicon atom, with the oxygen atoms at each vertex represented by dark grey spheres.

In a crystal, use of either the LDA or the GGA results in nearly identical coordinates,[55] perhaps because the strain on each bond is identical. In an amorphous sample, the strain is nonuniform and, therefore, the relaxation is nonuniform as well. The relative character of given silica tetrahedron sites in the lattice (as described by the deviation of the Si-O bond length and O-Si-O bond angles from their sample average) are similar for both LDA and GGA. It has been shown that gradient corrections are required to properly describe the relative energetics of different polymorphs of silica.[63] However, it has also been shown that LDA structure results for crystalline silica are closer to experiment than GGA results.[55] Other characterization is likely needed to understand which methods are best suited to study glass structure.

In all of the simulated glasses presented here (small and large), relaxation of the cell volume leads to an increase in density. Actual glass density can be lower due to inclusion of defects, and some bubbles and small voids, but these are expected to be minor contributions. Some factors that can contribute to higher densities include a possible bias due to the deliberate selection of only perfectly coordinated systems and that the finite size limits the possible population and spatial distributions of the ring sizes. It is well known that a small cutoff of the short-range interactions with a shift in the forces of the BKS potential leads to improved densities.[32] However, extended cutoffs or short cutoffs without shifting the forces lead to higher densities. This cutoff dependence is

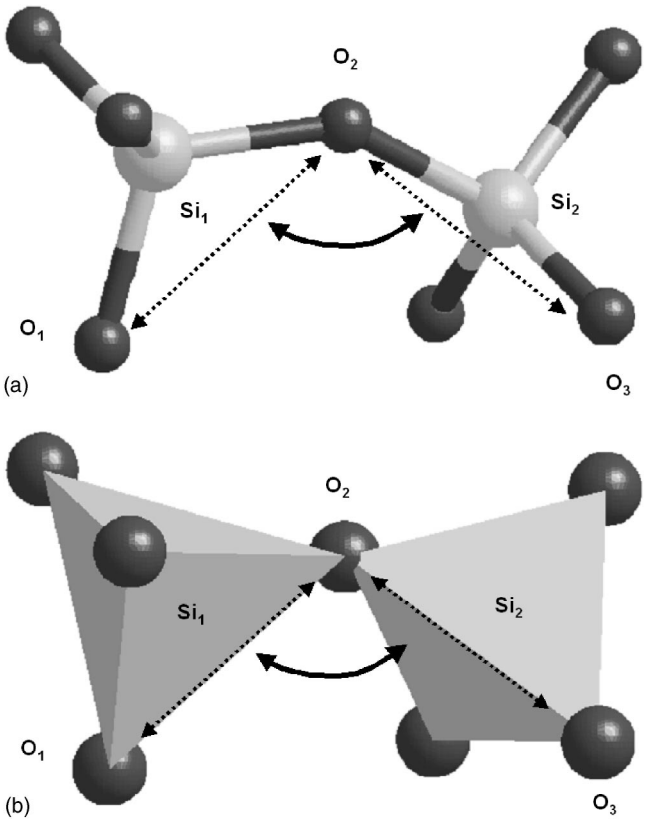

FIG. 16. Definition of tetrahedral tilt. The tilt is defined as the O-O-O angle between linked tetrahedra as shown in (a). The line between oxygen atoms that are bonded to the same silicon atom is an edge of a tetrahedron. The same angle is shown in the tetrahedral representation in (b).

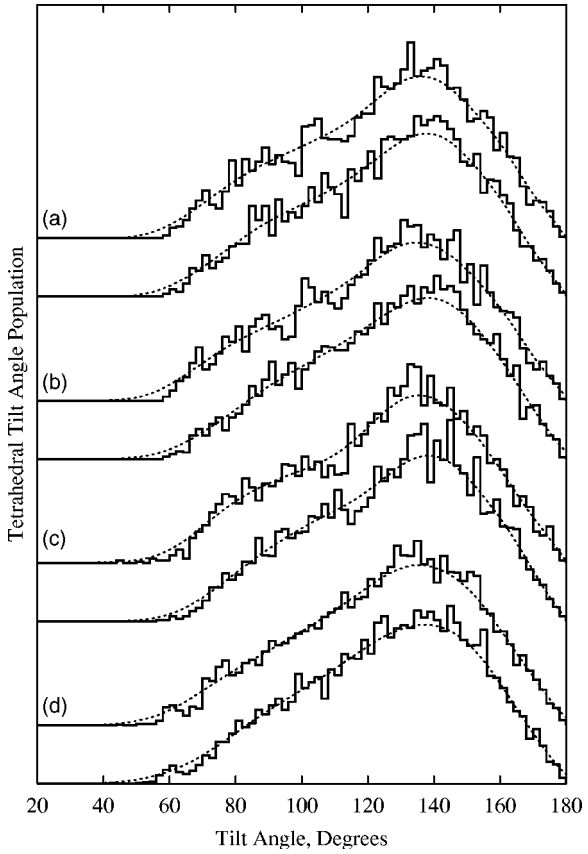

FIG. 17. Tetrahedral tilt distribution. Curves are presented in the same order as in Fig. 14. The dotted lines are a a guide to the eye.

also seen with the use of three-body potentials. In this work we see that the GGA leads to densities within the experimental density range as compared to the LDA or the BKS potential that have much higher densities. The trend in densities and bond lengths using the GGA and LDA for glass is similar to that determined for quartz.[55]

An alternative approach to overcome the size and statistical distribution limitations of a small glass system is to use an embedded method in which a small cluster of the entire system is calculated using an electronic structure method.[64] The rest of the system is treated by classical methods such that a Hamiltonian connecting the quantum and the classical regions is required to capture the effects of the extended structure in the quantum region. The most fundamental limitation is that the region of interest in which the electronic structure calculation will be carried out must be preselected. This last method is useful for more accurate calculations once structures where interesting chemistry and physics occur have been identified.

V. CONCLUSION

Analysis using several different measures of short- and medium-range order shows that an ensemble of ten samples with 72 ions each generated by classical dynamics simulations can provide a good statistical representation of structural features in fused silica. The structural analysis compared and contrasted results of simulations using an empirical potential energy function, the BKS potential, and DFT approaches, using either the LDA or GGA, applied to an ensemble of small samples with experimental data and simulations of much larger samples. Each structural characteristic investigated showed good agreement between the results obtained from simulations of the large system and the average of results from simulations of the small systems. In particular, the DFT results show more directional character of the Si-O bond than that obtained by the BKS potential, indicative of a covalent bond. On the basis of these data, it is concluded that it is possible to use several samples obtained from a small system with less than 100 ions to obtain local structural characteristics that are similar to those of a much larger system. Each small sample can be thought of as a small region in a much larger system.

ACKNOWLEDGMENTS

This work was supported by the Office of Basic Energy Science, Department of Energy and Semiconductor Research. The research was carried out at the University of Washington and at the William R. Wiley Molecular Sciences Laboratory, a national scientific user facility sponsored by the Department of Energy, Office of Biological and Environ-

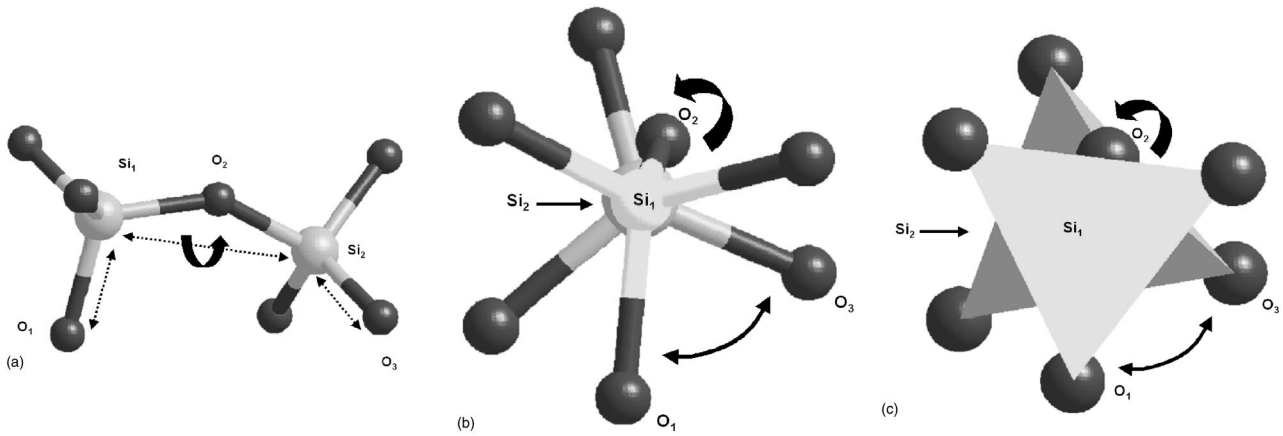

FIG. 18. Definition of tetrahedral twist. The twist between tetrahedra is defined as the torsion angle O-Si-Si-O, using the vector between neighboring silica tetrahedra as shown in (a). The view along the Si-Si axis is shown in (b) and (c) shows the same orientation in the tetrahedral representation.

mental Research located at the Pacific Northwest National Laboratory. Battelle operates the Pacific Northwest National Laboratory for the Department of Energy.

APPENDIX: SAMPLE SELECTION

The goal of the present study was an analysis of glass samples that are free of configuration defects. Some of the samples generated in the simulations, however, did not satisfy all criteria and were eliminated from the statistics presented here. Some of the samples were eliminated due to the presence of large voids and compressed regions within the simulation cell. While the void sizes found may be consistent with the structure of amorphous silica, the high density of the compressed region of the cell is not. These anomalous structures may be an artifact of the truncated BKS potential and the small cell size. Samples with this type of structure may have fully saturated bonds, and also have a total energy similar to more homogeneously distributed samples. These structures were identified visually. Figure 20 shows the void space of one of these inhomogeneous glasses with anomalous density fluctuations.

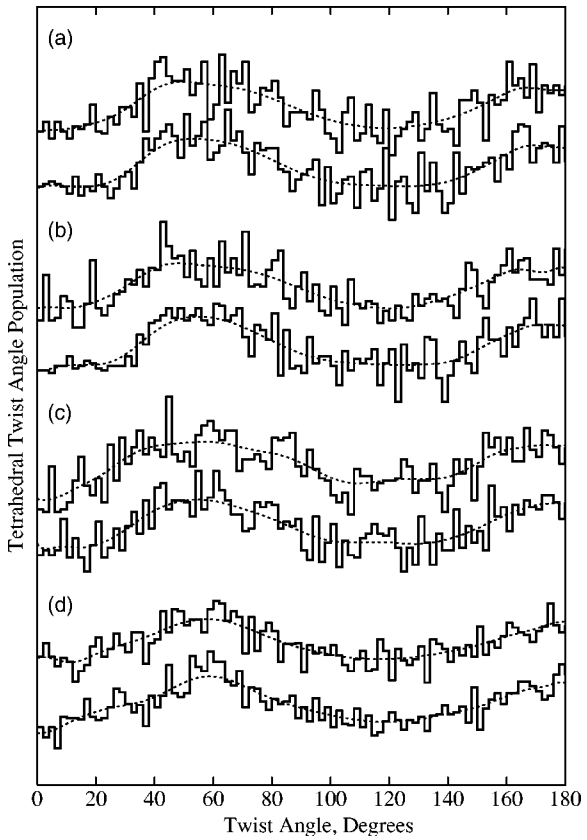

FIG. 19. Tetrahedral twist distribution. The dotted lines are a guide to the eye. Curves are presented in the same order as in Fig. 14.

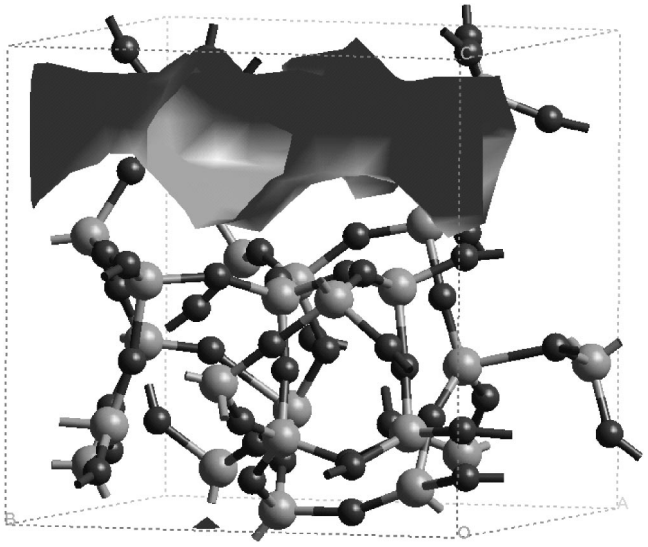

FIG. 20. Distribution of void space for a rejected glass sample. The larger, light gray spheres are silicon atoms. The smaller, dark gray spheres are oxygen atoms. The medium gray surface shows the void space accessible to a probe of diameter 1 Å. This sample is perfectly coordinated and has no edge-sharing tetrahedra, but the atoms are unusually closely packed into one part of the simulation cell, resulting in a large void.

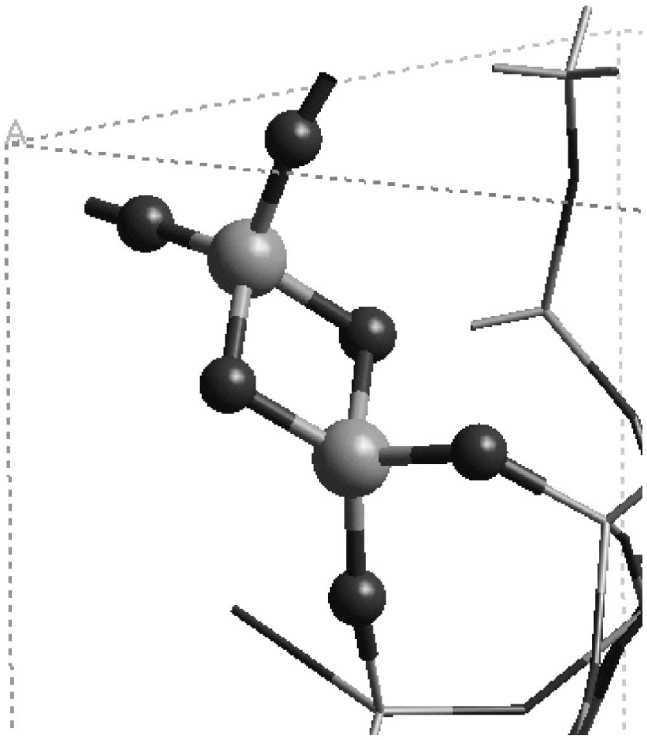

FIG. 21. Edge-sharing tetrahedra in silica. The larger, light gray spheres are silicon atoms. The smaller, dark gray spheres are oxygen atoms. This structure was found in one of the generated amorphous samples that was rejected for further use in this study. The two silicon atoms share two oxygen atoms, so that in the tetrahedral representation, the two silicon centers share an edge.

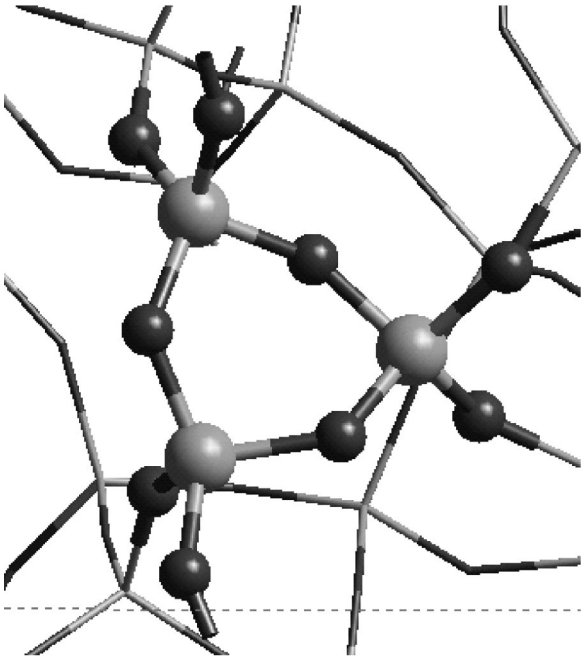

FIG. 22. The structure of a three-membered ring in silica. The color scheme is the same as for Fig. 21. This type of structure is nearly planar, with three silica tetrahedra forming a ring. The presence of three-rings in amorphous silica is detected by ir and Raman spectroscopy (Ref. 58). This type of structure is expected to occur with low probability, and the presence of three-rings is associated with increased reactivity and susceptibility to damage processes. One sample with three-rings was included in this study.

Another criterion for sample elimination was the presence of edge-sharing tetrahedra. This structure occurs when two silicon atoms share two oxygen atoms, as shown in Fig. 21.

The presence of several three-membered rings (more than two) was correlated with the presence of large voids, and thus was not a separate criterion for elimination. An example of a three-membered ring is shown in Fig. 22. Out of the 25 samples generated using the BKS potential, two were eliminated due to large void spaces, three due to coordination defects, and two due to the presence of an edge-sharing tetrahedron.

*Current address Sandia National Laboratories, Albuquerque, NM 87185-0196.

†Electronic address: hannes@u.washington.edu

‡Electronic address: rene.corrales@pnl.gov

[1] E. P. Gusev, in *Defects in* SiO_2 *and Related Dielectrics: Science and Technology*, edited by G. Pacchioni, L. Skuja, and D. Griscom, NATO Science Series (Kluwer Academic Press, Dordrecht, 2000), pp. 557–579.

[2] C. R. Kurkjian and D. M. Krol, in *Structure and Imperfections in Amorphous and Crystalline Silicon Dioxide*, edited by R. B. Devine, J.-P. Duraud, and E. Dooryheé (John Wiley and Sons, New York, 2000), pp. 449–474, and references therein.

[3] *Radioactive Waste Forms for the Future*, edited by W. Lutze and R. C. Ewing (North-Holland, Amsterdam, 1988).

[4] R. H. Doremus, *Glass Science* (John Wiley and Sons, New York, 1994).

[5] L. V. Woodcock, C. A. Angell, and P. Cheeseman, J. Chem. Phys. **65**, 1565 (1976).

[6] R. G. D. Valle and H. C. Andersen, J. Chem. Phys. **97**, 2682 (1992).

[7] J. Horbach, W. Kob, K. Binder, and C. A. Angell, Phys. Rev. E **54**, R5897 (1996).

[8] J. Sarnthein, A. Pasquarello, and R. Car, Phys. Rev. Lett. **74**, 4682 (1995).

[9] A. C. Wright, in *Defects in* SiO_2 *and Related Dielectrics: Science and Technology (Ref. 1)*, pp. 1–26.

[10] J. Sarnthein, A. Pasquarello, and R. Car, Phys. Rev. B **52**, 12690 (1995).

[11] M. Benoit, S. Ispas, and M. E. Tuckerman, Phys. Rev. B **64**, 224205 (2001).

[12] A. Pasquarello, J. Sarnthein, and R. Car, Phys. Rev. B **57**, 14133 (1998).

[13] A. Trave, P. Tangney, S. Scandolo, A. Pasquarello, and R. Car, Phys. Rev. Lett. **89**, 245504 (2002).

[14] A. Pasquarello and R. Car, Phys. Rev. Lett. **79**, 1766 (1997).
[15] A. Pasquarello and R. Car, Phys. Rev. Lett. **80**, 5145 (1998).
[16] A. Rahmani, M. Benoit, and C. Benoit, Phys. Rev. B **68**, 184202 (2003).
[17] D. R. Hamann, Phys. Rev. Lett. **81**, 3447 (1998).
[18] M. A. Szymanski, A. L. Shluger, and A. M. Stoneham, Phys. Rev. B **63**, 224207 (2001).
[19] J. Song, H. Jónsson, and L. R. Corrales, Nucl. Instrum. Methods Phys. Res. B **166–167**, 451 (2000).
[20] A. L. Shluger, J. L. Gavartin, M. A. Szymanski, and A. M. Stoneham, Nucl. Instrum. Methods Phys. Res. B **166–167**, 1 (2000).
[21] T. Bakos, S. N. Rashkeev, and S. T. Pantelides, Phys. Rev. Lett. **88**, 055508 (2002).
[22] M. Benoit, S. Ispas, P. Jund, and R. Jullien, Eur. Phys. J. B **13**, 631 (2000).
[23] B. W. H. van Beest, G. J. Kramer, and R. A. van Santen, Phys. Rev. Lett. **64**, 1955 (1990).
[24] A. Wright, A. Clare, D. Grimley, and R. N. Sinclair, J. Non-Cryst. Solids **112**, 33 (1989).
[25] A. C. Wright, J. Non-Cryst. Solids **106**, 1 (1988).
[26] W. Smith and T. Forester, J. Mol. Graphics **14**, 136 (1996).
[27] G. Kresse and J. Hafner, Phys. Rev. B **47**, R558 (1993).
[28] G. Kresse and J. Hafner, Phys. Rev. B **49**, 14251 (1994).
[29] G. Kresse and J. Furthmuller, Comput. Mater. Sci. **6**, 15 (1996).
[30] G. Kresse and J. Furthmuller, Phys. Rev. B **54**, 11169 (1996).
[31] X. Yuan and A. N. Cormack, J. Non-Cryst. Solids **283**, 69 (2001).
[32] K. Vollmayr, W. Kob, and K. Binder, Phys. Rev. B **54**, 15808 (1996).
[33] P. Ewald, Ann. Phys. **64**, 253 (1921).
[34] T. Koslowski, W. Kob, and K. Vollmayr, Phys. Rev. B **56**, 9469 (1997).
[35] B. Park and A. N. Cormack, J. Non-Cryst. Solids **255**, 112 (1999).
[36] B. Park, H. Li, and L. R. Corrales, J. Non-Cryst. Solids **297**, 220 (2002).
[37] N. T. Huff, E. Demilrap, T. Cagin, and W. A. Goddard III, J. Non-Cryst. Solids **253**, 133 (1999).
[38] D. R. Hamann, Phys. Rev. B **55**, 14784 (1997).
[39] W. Kohn and L. J. Sham, Phys. Rev. **140**, A1133 (1965).
[40] N. D. Mermin, Phys. Rev. **137**, A1441 (1965).
[41] J. P. Perdew and A. Zunger, Phys. Rev. B **23**, 5048 (1981).
[42] J. P. Perdew, J. A. Chevary, S. H. Vosko, K. A. Jackson, M. R. Pederson, D. J. Singh, and C. Fiolhais, Phys. Rev. B **46**, 6671 (1992).
[43] K. Laasonen, R. Car, C. Lee, and D. Vanderbilt, Phys. Rev. B **43**, 6796 (1991).
[44] N. Troullier and J. L. Martins, Phys. Rev. B **43**, 1993 (1991).
[45] D. Vanderbilt, Phys. Rev. B **41**, R7892 (1990).
[46] D. Vanderbilt, Phys. Rev. B **41**, R7892 (1990).
[47] S. Nosé, J. Chem. Phys. **81**, 511 (1984).
[48] D. Frenkel and B. Smit, *Understanding Molecular Simulation* (Academic Press, San Diego, CA, 1996).
[49] N. Mousseau and G. T. Barkema, Phys. Rev. E **57**, 2419 (1998).
[50] V. Lubchenko and P. G. Wolynes, Phys. Rev. Lett. **87**, 195901 (2001).
[51] H. J. C. Berendsen, J. P. M. Postma, W. F. Van Gunsteren, A. Di Nola, and J. R. Haak, J. Chem. Phys. **81**, 3684 (1984).
[52] A. N. Cormack, X. Yuan, and B. Park, Glass Phys. Chem. **27**, 28 (2001).
[53] X. Yuan and A. N. Cormack, J. Non-Cryst. Solids **319**, 31 (2003).
[54] A. C. Wright, J. Non-Cryst. Solids **159**, 264 (1993).
[55] T. Demuth, Y. Jeanvoine, J. Hafner, and J. G. Ángyán, J. Phys.: Condens. Matter **11**, 3833 (1999).
[56] X. Yuan and A. N. Cormack, Comput. Mater. Sci. **24**, 343 (2002).
[57] X. Yuan, V. Pulim, and L. W. Hobbs, J. Nucl. Mater. **289**, 71 (2001).
[58] F. L. Galeener, J. Non-Cryst. Solids **49**, 53 (1982).
[59] J. Chan, T. Huser, S. Risbud, and D. Krol, Appl. Phys. A: Mater. Sci. Process. **76**, 367 (2003).
[60] W. L. Warren, P. M. Lenahan, and C. J. Brinker, Solid State Commun. **79**, 137 (1991).
[61] A. E. Geissberger and F. L. Galeener, Phys. Rev. B **28**, 3266 (1983).
[62] E. Chagarov, J. B. Adams, and J. Kieffer, Modell. Simul. Mater. Sci. Eng. **12**, 337 (2004).
[63] D. R. Hamann, Phys. Rev. Lett. **76**, 660 (1996).
[64] A. S. Mysovsky, P. V. Sushko, S. Mukhopadhyay, A. H. Edwards, and A. L. Shluger, Phys. Rev. B **69**, 085202 (2004).